

Anomalous single production of fourth family up type quark associated with neutral gauge bosons at the LHC

O. Çakır*

Department of Physics, Ankara University, 06100, Ankara, Turkey

I.T. Çakır†

Department of Physics, CERN, 1211, Geneva 23, Switzerland

A. Senol‡ and A.T. Tasci§

Department of Physics, Kastamonu University, 37100, Kastamonu, Turkey

Abstract

From the present limits on the masses and mixings of fourth family quarks, they are expected to have mass larger than the top quark and allow a large range of mixing of the third family. They could also have different dynamics than the quarks of three families of the Standard Model. The single production of the fourth family up type quark t' has been studied via anomalous production process $pp \rightarrow t'VX$ (where $V = g, Z, \gamma$) at the LHC with the center of mass energy of 7 and 14 TeV. The signatures of such process are discussed within both the SM decay modes and anomalous decay modes of t' quarks. The sensitivity to anomalous coupling $\kappa/\Lambda = 0.004 \text{ TeV}^{-1}$ can be reached at $\sqrt{s} = 14 \text{ TeV}$ and $L_{int} = 100 \text{ pb}^{-1}$.

PACS numbers:

12.60.-i Models beyond the standard model

14.65.Jk Other quarks (e.g., 4th generations)

13.85.Rm Limits on production of particle

*Electronic address: ocakir@science.ankara.edu.tr

†Electronic address: tcakir@mail.cern.ch

‡Electronic address: asenol@kastamonu.edu.tr

§Electronic address: atasci@kastamonu.edu.tr

I. INTRODUCTION

The number of fermion families in the Standard Model (SM) and its very extensions remain arbitrary. There is a number of experimental discrepancies with the SM expectations at some level of standard deviations, and they can also be interpreted as the loop effects or the flavor changing neutral current (FCNC) effects by the fourth family fermions. A minimal framework can give rise to FCNC effects through exchange of massive SM bosons whose couplings to the light fermions get modified by mixing with the fourth family fermions. It is also important to interpret the low energy measurements for the contributions from extra fermions and analyze them in view of the latest electroweak precision data [1, 2].

The current limits on the masses of the fourth SM family leptons are [3]: $m_{\nu'} > 100$ GeV, $m_{\nu'} > 90$ (80) GeV for Dirac (Majorana) neutrinos. Recently, the Collider Detector at Fermilab (CDF) has constrained the masses of the fourth SM family quarks: $m_{t'} > 335$ GeV at 95% CL. [4], $m_{b'} > 338$ GeV at 95% CL. [5]. On the other hand, the perturbativity of the Yukawa coupling implies that $m_{t'} \leq 600$ GeV, and the arguments based on the partial wave unitarity restrict to an upper bound $m_{t'} \approx 500$ GeV [6]. The parameter space of fourth family fermion masses with minimal contributions to the oblique parameters S and T , and in agreement with all experimental constraints, leads to a quark mass splitting $m_{t'} - m_{b'} \simeq 50 + 10 \ln(m_h/115\text{GeV})$ [7], where m_h is the mass of Higgs boson. The heavy quark mass bounds may be relaxed if they are considered together with the fourth family leptons, which could help in the partial cancellation of the effect of fourth family on the S and T parameters. Even in the assumption of the absence of this cancellation the precision measurements restrict $m_{t'} - m_{b'} \approx 50 - 100$ GeV. A review of theoretical and experimental motivations can be found in [8].

If the fourth family quarks are discovered at the LHC, it is expected that it plays a crucial role solving some of the currently open questions such as the CP violation and flavor structure of the standard theory [9–15], electroweak symmetry breaking [16–19], hierarchies of fermion mass spectrum and mixing angle in quark/lepton sectors [20–23]. The fourth family quark masses and mixings can be predicted in the allowed parameter space which is in the reach of the LHC. In the four families scenario, the assumption of the unitarity of 4×4 mixing matrix holds and it allows a large range of the elements as far as the magnitudes and phases of the V_{tq} are concerned. A serious contribution can be expected for the production

of the fourth family fermions from the anomalous interactions. These effects of the fourth family quarks have been studied in detail at future linear colliders [24], ep colliders [25, 26], and recently at hadron colliders [27]. The anomalous resonant production of fourth family up type quarks via $gq_i \rightarrow t'$ ($q_i = u, c$) subprocess [28, 29] and single production of fourth family quarks [30] have been studied at the LHC.

In this study, we investigate the production of fourth family up type quark (t') with the association of the gauge bosons (g, Z, γ) through anomalous interactions at the LHC. Then, we consider t' decays into SM and anomalous modes for some relevant parameter space. We discuss the decay modes for some parameter space and the t' signal observability at three different energies 7 and 14 TeV.

II. INTERACTIONS WITH FOURTH FAMILY QUARKS

The interaction Lagrangian for the fourth family quarks ($Q' = t', b'$) within the SM is given by

$$\begin{aligned}
L_S = & -g_e \sum_{Q'_i=t',b'} Q_{q_i} \bar{Q}'_i \gamma^\mu Q'_i A_\mu - g_s \sum_{Q'_i=t',b'} \bar{Q}'_i T^a \gamma^\mu Q'_i G_\mu^a \\
& - \frac{g_z}{2} \sum_{Q'_i=t',b'} \bar{Q}'_i \gamma^\mu (g_v^i - g_a^i \gamma_5) Q'_i Z_\mu \\
& - \frac{g_e}{2\sqrt{2} \sin \theta_w} \sum_{Q'_i=t',b'} V_{ij} \bar{Q}'_i \gamma^\mu (1 - \gamma_5) q_j W_\mu^\pm + \text{H.c.}
\end{aligned} \tag{1}$$

where A_μ , G_μ , Z_μ and W_μ^\pm are the fields for photon, gluon, Z -boson and W^\pm bosons, respectively. $T_a = \lambda_a/2$ are Gell-Mann matrices; Q_q is the charge of the quark; g_e , g_z and g_s are the electromagnetic, weak neutral-current and strong coupling constants, respectively. The coupling $g_z = g_e/\sin \theta_W \cos \theta_W$ where θ_W is the Weinberg angle. The g_v and g_a are the vector and axial-vector couplings of the neutral weak current with fourth family quarks. The elements of the extended CKM mixing matrix are presented by V_{ij} . The effective Lagrangian for the FCNC anomalous interactions between the fourth family quarks, ordinary quarks and the gauge bosons V (g, Z, γ) can be written as follows

$$L_A = \sum_{q_i=u,c,t} \frac{\kappa_\gamma^{q_i}}{\Lambda} Q_{q_i} g_e \bar{t}' \sigma_{\mu\nu} q_i F^{\mu\nu} + \sum_{q_i=u,c,t} \frac{\kappa_z^{q_i}}{2\Lambda} g_z \bar{t}' \sigma_{\mu\nu} q_i Z^{\mu\nu}$$

Table I: The branching ratios BR(%) and total decay widths (Γ) of t' quark depending on the mass ($m_{t'}$), here we take the anomalous coupling $\kappa/\Lambda = 0.1(1) \text{ TeV}^{-1}$.

BR(%) \leftrightarrow $m_{t'}(\text{GeV}) \downarrow$	Wb	Ws	Wd	gu/gc	gt	Zu/Zc	Zt	$\gamma u/\gamma c$	γt	$\Gamma(\text{GeV})$
300	72.00(7.40)	19.00(2.00)	0.02(0.003)	3.60(37.00)	1.00(11.00)	0.22(2.20)	0.02(0.24)	0.08(0.82)	0.02(0.24)	0.59(5.75)
400	71.00(6.80)	19.00(1.80)	0.03(0.003)	3.50(33.00)	1.90(18.00)	0.23(2.20)	0.10(0.95)	0.08(0.74)	0.04(0.39)	1.43(15.02)
500	71.00(6.40)	19.00(1.70)	0.03(0.003)	3.50(32.00)	2.30(21.00)	0.23(2.10)	0.15(1.30)	0.08(0.70)	0.05(0.48)	2.82(30.98)
600	71.00(6.20)	19.00(1.70)	0.03(0.003)	3.50(31.00)	2.60(23.00)	0.23(2.10)	0.17(1.50)	0.08(0.68)	0.06(0.52)	4.89(55.27)
700	70.00(6.10)	19.00(1.60)	0.03(0.003)	3.40(30.00)	2.80(25.00)	0.24(2.10)	0.19(1.70)	0.08(0.67)	0.06(0.55)	7.78(89.52)
800	70.00(6.00)	19.00(1.60)	0.03(0.003)	3.40(30.00)	3.00(26.00)	0.24(2.00)	0.20(1.70)	0.08(0.66)	0.07(0.57)	11.64(135.40)

$$\begin{aligned}
& + \sum_{q_i=u,c,t} \frac{\kappa_g^{q_i}}{\Lambda} g_s \bar{t}' \sigma_{\mu\nu} T_a q_i G_a^{\mu\nu} + h.c. \\
& + \sum_{q_i=d,s,b} \frac{\kappa_\gamma^{q_i}}{\Lambda} Q_{q_i} g_e \bar{b}' \sigma_{\mu\nu} q_i F^{\mu\nu} + \sum_{q_i=d,s,b} \frac{\kappa_z^{q_i}}{2\Lambda} g_z \bar{b}' \sigma_{\mu\nu} q_i Z^{\mu\nu} \\
& + \sum_{q_i=d,s,b} \frac{\kappa_g^{q_i}}{\Lambda} g_s \bar{b}' \sigma_{\mu\nu} T_a q_i G_a^{\mu\nu} + h.c. \tag{2}
\end{aligned}$$

where $F_{\mu\nu}$, $Z_{\mu\nu}$, and $G_{\mu\nu}$ are the field strength tensors of the photon, Z boson and gluons, respectively; the κ_γ , κ_z and κ_g define the strength of the anomalous couplings for the neutral currents with the photon, Z boson and gluon, respectively. Λ is the scale for new physics. We have implemented both the SM and anomalous interaction vertices for the fourth family quarks into the CompHEP [31] and we use parton distribution library CTEQ6M [32] with the factorization scale $Q = m_{t'}$.

Here, we have used the parametrization in which the values for the elements $|V_{t'd}| = 0.0044$, $|V_{t'b}| = 0.22$ and $|V_{t's}| = 0.114$ are given by Ref. [33]. In order to reduce free parameters we assume that the anomalous couplings κ_z^q , κ_g^q and κ_γ^q are equal to κ . The analytical expressions for the decay widths of t' quark both in SM and anomalous modes are given in Ref. [28]. The branching ratios into both SM and anomalous decay modes are given in Table I. It is seen from Table I that the anomalous decay mode of the $t' \rightarrow qg$ is dominant for $\kappa/\Lambda = 1 \text{ TeV}^{-1}$.

The Feynman diagrams for the single production of t' quark together with the vector boson V (g, Z, γ) are presented in Fig. 1. Here, the last two diagrams are relevant only for the $t'g$ production process. The analytical expressions of the differential cross sections for the subprocess $qg \rightarrow t'V$ ($V = g, Z, \gamma$) are calculated and given in the Appendix.

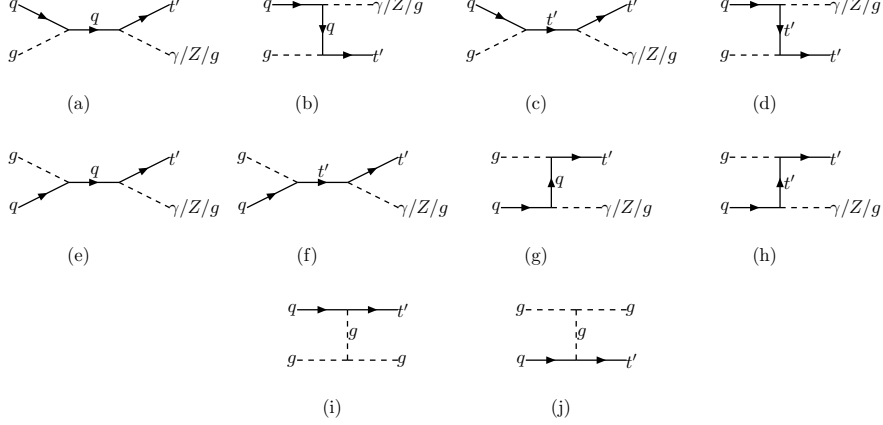


Figure 1: Feynman diagrams for anomalous $t'V$ ($V = g, Z, \gamma$) production at the LHC.

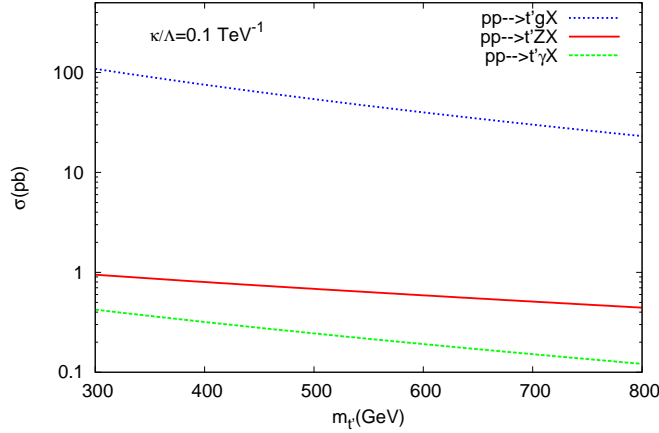


Figure 2: The cross sections for anomalous $t'V$ ($V = g, Z, \gamma$) production at the LHC with 14 TeV.

III. NUMERICAL CALCULATIONS

The total cross sections for the $t'V$ ($V = g, Z, \gamma$) production with $\kappa/\Lambda = 0.1 \text{ TeV}^{-1}$ are presented in Fig. 2 depending on the mass $m_{t'}$ at the collision center of mass energy of 14 TeV. As seen from Fig. 2 the cross section for the process $pp \rightarrow t'gX$ is much larger than that of the $pp \rightarrow t'\gamma X$ and $pp \rightarrow t'ZX$ processes. Due to large QCD background in the qgq production (which includes only one type anomalous coupling κ_g for the case $t' \rightarrow W^+q$) and small branching ratio into $q\gamma/Z$ for $\kappa/\Lambda \leq 0.1 \text{ TeV}^{-1}$ as seen from Table I, we consider only the processes $pp \rightarrow t'ZX$ and $pp \rightarrow t'\gamma X$ with subsequent decay into SM mode $t' \rightarrow W^+b$ for both processes, and the anomalous mode $t' \rightarrow tg$ for the first process. Hereafter, in the numerical calculations we use the anomalous coupling $\kappa/\Lambda = 0.1 \text{ TeV}^{-1}$.

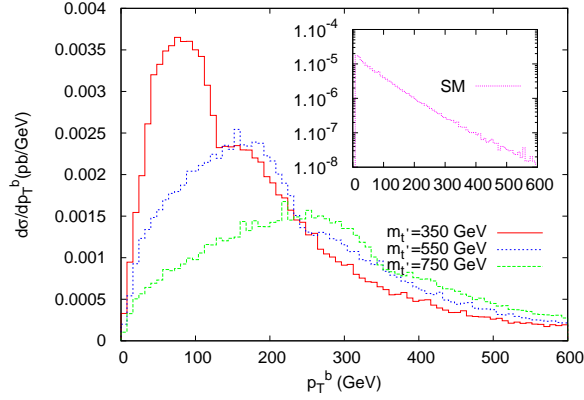


Figure 3: The p_T distributions of b quark from signal and background process $pp \rightarrow W^+ b Z X$ at $\sqrt{s}=14$ TeV.

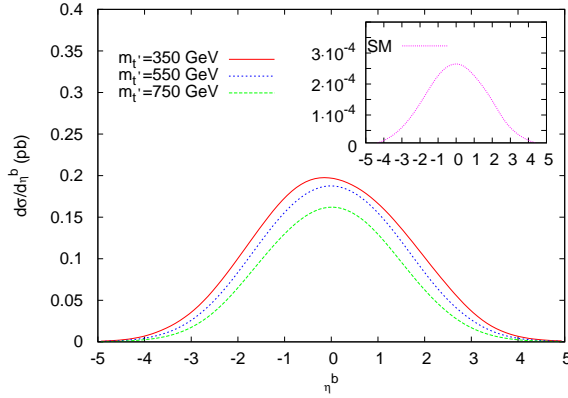


Figure 4: The η distributions of b quark from signal and background process $pp \rightarrow W^+ b Z X$ at $\sqrt{s}=14$ TeV.

Transverse momentum distributions of the b quark for the signal $pp \rightarrow W^+ b Z X$ (where $m_{t'} = 350, 550, 750$ GeV) and the SM background are shown in Fig. 3. The signal differential cross sections show peak around $p_T = 75, 150$ and 250 GeV for the values of $m_{t'} = 350, 550$ and 750 GeV, respectively. The background differential cross section smoothly decreases with respect to the p_T of b quark. The rapidity distributions of the b quark from the signal and background locate mostly in the range of $|\eta^b| < 2$ as shown in Fig. 4. The signal has peak around the t' mass values of $350, 550$ and 750 GeV over the smooth background. The level of the relevant background is compared with the signal in the invariant mass distributions of $W^+ b$ system as shown in Fig. 5.

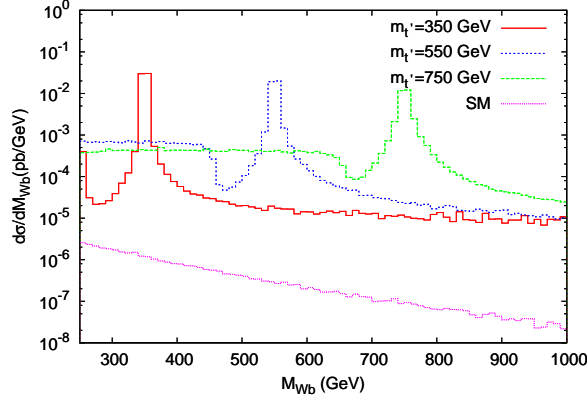


Figure 5: Invariant mass distributions of the W^+b system ($pp \rightarrow W^+bZX$) for the given parametrization at $\sqrt{s}=14$ TeV.

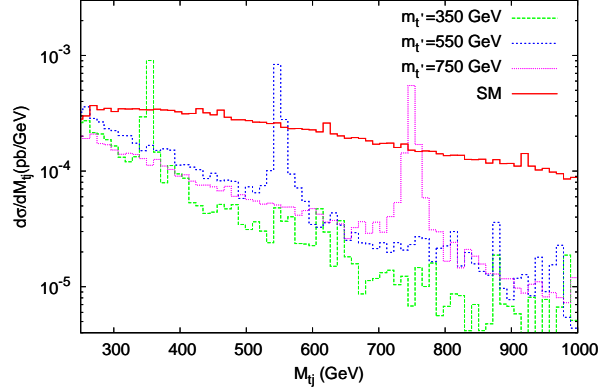


Figure 6: Invariant mass distributions of the $t + jet$ system ($pp \rightarrow tgZX$ for signal and $pp \rightarrow tjZX$ for background) at $\sqrt{s}=14$ TeV.

The differential cross sections for the signal process $pp \rightarrow tgZX$ in the tg invariant mass distributions are given in Fig. 6. The signal shows itself as the peaks around the assumed mass values of $m_{t'}$. Here, we take into account the process $pp \rightarrow tjZX$ for background where j denotes light quarks in the final state.

The p_T distributions of the photon from the signal and background processes $pp \rightarrow W^+b\gamma X$ are shown in Fig. 7.

In order to calculate the statistical significance (SS) we use the following formula

$$SS = \sqrt{2[(S + B) \ln(1 + S/B) - S]}$$

where S and B are the number of events of the signal and background, respectively. In

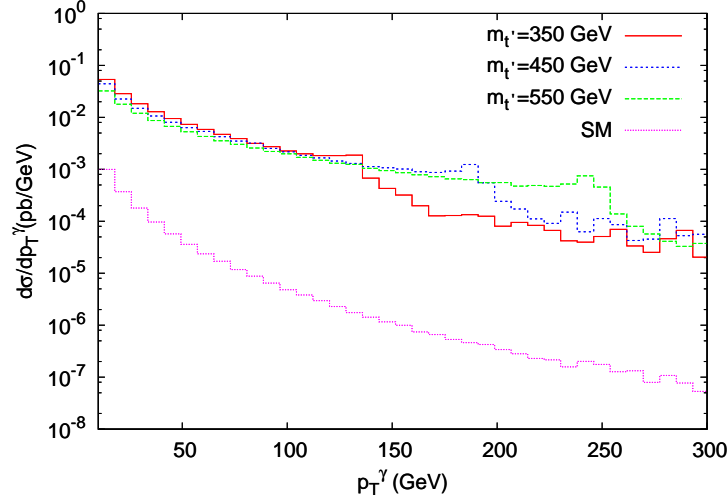


Figure 7: The p_T distributions of photon from the signal and background at $\sqrt{s} = 14$ TeV.

the analysis, we use the kinematical cuts on the transverse momentum $p_T^j > 50$ GeV of jets and $p_T^\gamma > 20$ GeV of photons. We calculate the signal and background cross sections for the process $pp \rightarrow W^+b(Z, \gamma)X$ in the invariant mass interval satisfying the conditions $|m_{t'} - M_{Wb}| < 10$ GeV for the t' mass range 300-500 GeV and $|m_{t'} - M_{Wb}| < 20$ GeV for the t' mass range 500-800 GeV. In the significance calculations for the signal process $pp \rightarrow W^+b(Z, \gamma)X$, we take into account the hadronic W -decay and leptonic Z -decay. We use b -tagging efficiency as 0.5 for considered processes.

The SS values, total cross sections of the signal and background process $pp \rightarrow W^+bZ(\gamma)X$ are given in Table II(IV) for $\sqrt{s}=14$ TeV and $L = 10^5$ pb $^{-1}$, and in Table III(V) for $\sqrt{s}=7$ TeV and $L = 10^3$ pb $^{-1}$, respectively.

In Tables VI and VII, we consider leptonic (hadronic) decays of Z -boson and hadronic (leptonic) decays of W -boson for the process $pp \rightarrow tjZX$. The conditions $|m_{t'} - M_{tj}| < 10$ GeV for $m_{t'} = 300$ -500 GeV and $|m_{t'} - M_{tj}| < 20$ GeV for $m_{t'} = 500$ -800 GeV are used for the process $pp \rightarrow tjZX$. Taking the integrated luminosity $L = 10^5$ pb $^{-1}$, the SS values and the total cross sections of the signal and background are given in Table VI for $\sqrt{s}=14$ TeV.

In Fig. 8, we plot the contours for different mass values, namely $m_{t'} = 350, 450$ and 550 GeV, with the 3σ significance for process $pp \rightarrow W^+bZX$. We find that the lower limit on the anomalous couplings κ_g/Λ and κ_z/Λ can be as low as 0.015 and 0.0035 TeV $^{-1}$, respectively.

In Fig. 9, we plot the contours for the mass values $m_{t'} = 350, 450$ and 550 GeV for 3σ

Table II: The total cross sections of the signal and background process $pp \rightarrow W^+bZX$, as well as the SS values at $\sqrt{s}=14$ TeV with $L = 10^5\text{pb}^{-1}$.

$m_{t'}$ (GeV)	$10^{-5} \times \sigma_B(\text{pb})$	$10^{-1} \times \sigma_S(\text{pb})$	SS
300	4.85	6.70	165
400	2.21	5.42	153
500	1.05	4.38	142
600	1.10	3.82	131
700	0.62	3.15	121
800	0.37	2.56	111

Table III: The same as Table II, but for $\sqrt{s}=7$ TeV and $L = 10^3\text{pb}^{-1}$.

$m_{t'}$ (GeV)	$10^{-6} \times \sigma_B(\text{pb})$	$10^{-1} \times \sigma_S(\text{pb})$	SS
300	8.54	1.23	7.1
400	3.56	0.86	6.1
500	1.56	0.62	5.3
600	1.50	0.47	4.6
700	0.77	0.34	4.0
800	0.41	0.25	3.4

significance. It is found that lower limit on the anomalous couplings κ_g/Λ and κ_γ/Λ from the process $pp \rightarrow W^+b\gamma X$ can be as low as 0.004 and 0.025 TeV^{-1} , respectively.

IV. CONCLUSIONS

The anomalous FCNC interactions could be important for some parameter regions due to the expected large masses of the fourth family quarks. From the analysis of single production of t' quark associated with the neutral gauge bosons the sensitivity to the (κ_g, κ_z) and $(\kappa_g, \kappa_\gamma)$ can be obtained as low as (0.015, 0.0035) and (0.004, 0.025) at the LHC with the center of mass energy of 14 TeV and the integrated luminosity of 10^5pb^{-1} .

Table IV: The SS values, total cross sections of the signal and background process $pp \rightarrow t\gamma ZX$ at $\sqrt{s}=14$ TeV with $L = 10^5 \text{pb}^{-1}$.

$m_{\nu'}$ (GeV)	$10^{-6} \times \sigma_B(\text{pb})$	$10^{-1} \times \sigma_S(\text{pb})$	SS
300	24.6	2.68	389
400	9.87	3.12	446
500	4.43	3.03	457
600	4.36	2.75	434
700	2.26	2.51	426
800	1.25	2.28	415

Table V: The same as Table IV, but for $\sqrt{s}=7$ TeV and $L = 10^3 \text{pb}^{-1}$.

$m_{\nu'}$ (GeV)	$10^{-7} \times \sigma_B(\text{pb})$	$10^{-2} \times \sigma_S(\text{pb})$	SS
300	43.5	7.45	21.1
400	15.5	8.30	23.6
500	6.18	7.42	23.2
600	5.17	6.13	21.1
700	2.44	5.05	19.7
800	1.19	4.03	17.9

Table VI: The total cross sections of the signal and background process $pp \rightarrow tgZX$ and SS values which corresponds to the leptonic (hadronic) decays of Z -boson and hadronic (leptonic) decays of W -boson at $\sqrt{s}=14$ TeV with $L = 10^5 \text{pb}^{-1}$.

$m_{\nu'}$ (GeV)	$10^{-3} \times \sigma_B(\text{pb})$	$10^{-3} \times \sigma_S(\text{pb})$	SS
300	0.75	7.94	8.0(14.3)
350	1.43	11.0	8.7(15.7)
400	2.19	12.3	8.5(15.2)
500	3.85	12.2	7.1(12.8)
600	5.46	12.2	6.4(11.5)
700	6.94	10.4	5.1(9.2)
800	8.18	8.60	4.1(7.3)

Table VII: The same as Table VI, but for $\sqrt{s}=7$ TeV.

$m_{t'}$ (GeV)	$10^{-4} \times \sigma_B$ (pb)	$10^{-3} \times \sigma_S$ (pb)	SS
300	1.82	1.52	3.3(5.9)
350	3.20	2.00	3.5(6.3)
400	4.59	2.06	3.3(5.9)
500	7.14	1.76	2.5(4.5)
600	8.96	1.55	2.1(3.7)
700	10.1	1.15	1.5(2.8)
800	10.6	0.84	1.1(2.0)

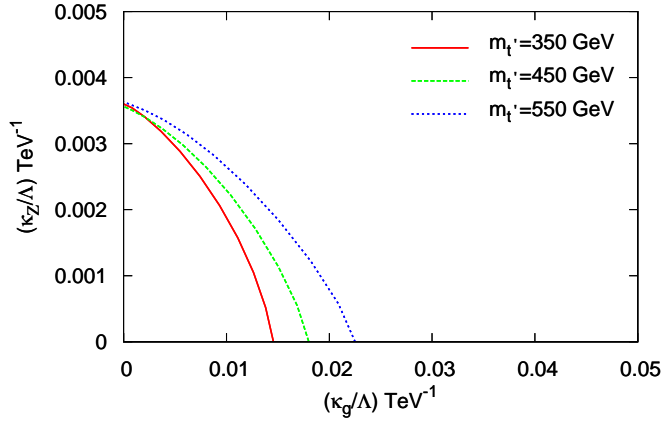


Figure 8: The 3σ contour plot for the signal observability at $\sqrt{s} = 14$ TeV and $L = 10^5$ pb $^{-1}$.

APPENDIX

The differential cross section for the subprocess $qg \rightarrow t'\gamma$ is given as

$$\begin{aligned}
 \frac{d\hat{\sigma}}{d\hat{t}}(qg \rightarrow t'\gamma) = & \frac{2\pi\alpha_s\alpha}{27\hat{s}^2\Lambda^2} \left\{ \frac{\kappa_g^2 2\hat{s}[m^2(m^2 - 6\hat{s}) + \hat{s}^2]}{[(\hat{s} - m^2)^2 + \Gamma^2 m^2]} + \frac{2\kappa_\gamma^2(m^2 - \hat{s})^2}{\hat{s}} + \kappa_g\kappa_\gamma \left[-(\hat{s} + m^2) \right. \right. \\
 & + \left. \frac{3(2\hat{s}^3 - m^6) - m^2[2\hat{s}(\hat{s} - 8m^2) + \hat{t}(3m^2 - \hat{s})]}{[(\hat{s} - m^2)^2 + \Gamma^2 m^2]} \right] + 2 \left[\frac{\kappa_\gamma^2 \hat{t}[m^2(\hat{u} - 2\hat{t}) - \hat{t}\hat{u}]}{(\hat{t} - m^2)^2} \right. \\
 & \left. \left. + \frac{\kappa_g^2 \hat{u}(m^2 - \hat{t})}{\hat{t}} - \frac{\kappa_g\kappa_\gamma [3m^4 + (3\hat{u} - 7\hat{t})m^2 + \hat{t}(4\hat{t} - \hat{u})]}{4(\hat{t} - m^2)} \right] + [\hat{t} \leftrightarrow \hat{u}] \right\}
 \end{aligned}$$

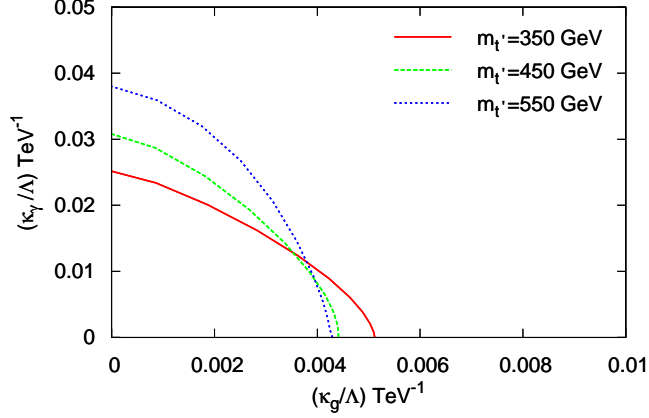


Figure 9: The same as Fig. 8, but for the anomalous couplings κ_γ/Λ vs κ_g/Λ .

$$\begin{aligned}
& + \left[\frac{\kappa_\gamma^2}{\hat{s}(\hat{t}-m^2)(\hat{u}-m^2)} + \frac{\kappa_g^2 \hat{s}}{\hat{u}\hat{t}[(\hat{s}-m^2)^2 + \Gamma^2 m^2]} \right] [m^2(\hat{s}-m^2)[m^2(\hat{s}-m^2) + 2\hat{u}\hat{t}] \\
& + \frac{\kappa_\gamma \kappa_g (\hat{s}-m^2)}{[(\hat{s}-m^2)^2 + \Gamma^2 m^2]} \left[\frac{3m^4(\hat{u}-m^2) + 3(\hat{s}^2 + 3\hat{s}\hat{t} + \hat{t}^2)m^2 + \hat{s}\hat{t}\hat{u}}{(\hat{t}-m^2)} \right. \\
& \left. + \frac{3m^4(\hat{t}-\hat{s}) - 3(\hat{s}^2 + \hat{s}\hat{t} - \hat{t}^2)m^2 + \hat{s}\hat{t}\hat{u}}{(\hat{u}-m^2)} \right] \Big\} \quad (3)
\end{aligned}$$

where \hat{s} , \hat{t} and \hat{u} are the Mandelstam variables for the subprocess; m and Γ denote the mass and decay width of t' quark, respectively. The strong and electromagnetic coupling constants are presented by α_s and α , respectively. The differential cross section for the subprocess $qg \rightarrow t'g$ is given as

$$\begin{aligned}
\frac{d\hat{\sigma}}{d\hat{t}}(qg \rightarrow t'g) & = \frac{\pi\alpha_s^2\kappa_g^2}{72\hat{s}^2\Lambda^2} \left\{ \frac{32\hat{s}[m^2(m^2-6\hat{s}) + \hat{s}^2]}{[(\hat{s}-m^2)^2 + \Gamma^2 m^2]} + \frac{32(m^2-\hat{s})^2}{\hat{s}} + 2(m^2+\hat{s}) \right. \\
& + \frac{144(m^2-\hat{s})^3}{[(\hat{s}-m^2)^2 + \Gamma^2 m^2]} + \frac{9[16m^6 + 18m^4(\hat{s}-m^2) + 2m^2(\hat{u}^2 + \hat{t}^2) + 3\hat{u}\hat{t}(5m^2 + \hat{s})]}{\hat{t}\hat{u}} \\
& + 4 \left[\frac{8[m^2(\hat{u}-2\hat{t}) - \hat{t}\hat{u}]}{(\hat{t}-m^2)^2} + \frac{9[4\hat{t}\hat{s} + \hat{u}(3m^2 + \hat{u}) - 4m^4] + 8(m^2 - \hat{t})\hat{u}}{\hat{t}} \right. \\
& + \frac{9[8m^6 - 6(2\hat{s} + \hat{u})m^4 + 4\hat{s}^2(m^2 - \hat{u}) + 9\hat{s}\hat{u}m^2 - \hat{u}^2(2m^2 - \hat{s})]}{4\hat{s}\hat{u}} \\
& + \frac{8[3m^4 + (3\hat{u} - 7\hat{t})m^2 + \hat{t}(4\hat{t} - \hat{u})]}{\hat{t}-m^2} + \frac{4m^2}{\hat{s}} \left[\frac{(m^2-\hat{s})\hat{t}}{\hat{t}-m^2} + \frac{\hat{s}^2(m^2-\hat{u})(\hat{s}-m^2)}{\hat{t}[(\hat{s}-m^2)^2 + \Gamma^2 m^2]} \right] \\
& \left. + \frac{[3(m^2-\hat{u})m^4 + (\hat{t}-3m^2)\hat{s}^2 + (\hat{s}-3m^2)\hat{t}^2 - 10\hat{t}\hat{s}m^2](\hat{s}-m^2)}{(\hat{t}-m^2)[(\hat{s}-m^2)^2 + \Gamma^2 m^2]} \right] + [\hat{t} \leftrightarrow \hat{u}] \Big\} \quad (4)
\end{aligned}$$

$$\begin{aligned}
& + \left[\frac{9[(5\hat{t} - 4\hat{s})m^4 - 4\hat{s}^2(\hat{t} + m^2) - 3\hat{t}\hat{s}m^2 + \hat{t}^2(\hat{s} - 5m^2)](\hat{s} - m^2)}{\hat{t}[(\hat{s} - m^2)^2 + \Gamma^2 m^2]} + [\hat{s} \leftrightarrow \hat{u}] \right] \\
& + \left[\frac{9[(5\hat{t} - \hat{s})m^4 + 6\hat{s}^2(\hat{t} - 2m^2) + \hat{t}^2(\hat{s} - 5m^2) + \hat{s}(5\hat{s}^2 - 9\hat{t}m^2)](\hat{s} - m^2)}{\hat{u}[(\hat{s} - m^2)^2 + \Gamma^2 m^2]} \right] \\
& + [\hat{s} \leftrightarrow \hat{u}] \Big] \Big\}
\end{aligned}$$

The differential cross section for the subprocess $qg \rightarrow t'Z$ is given as

$$\begin{aligned}
\frac{d\hat{\sigma}}{d\hat{t}}(qg \rightarrow t'Z) &= \frac{\pi\alpha_s\alpha}{432\hat{s}^2\Lambda^2 s_W^2 c_W^2} \left\{ \frac{\kappa_g^2 \hat{s}}{m_Z^2 [(\hat{s} - m^2)^2 + \Gamma^2 m^2]} [18(g_v^2 + g_a^2)(m^6 + m^4(m_Z^2 - \hat{s})) \right. \\
& - 2m_Z^4(\hat{s} + m^2) + \hat{s}^2(m_Z^2 - m^2 + \hat{s}) + 2\hat{s}m^2 m_Z^2 (-160s_W^4 + 120s_W^2 + 9)] \\
& + \frac{36\kappa_z^2}{\hat{s}} [2m^4 - m_Z^2(\hat{s} + m^2 + m_Z^2) + 2\hat{s}(\hat{s} - 2m^2)] \\
& + \frac{324g_v\kappa_z\kappa_g(\hat{s} - m^2)}{[(\hat{s} - m^2)^2 + \Gamma^2 m^2]} [m_Z^2(\hat{s} + m^2) - \hat{s}(\hat{s} - 2m^2) - m^4] \\
& + 36 \left[\frac{\kappa_z^2}{(\hat{t} - m^2)^2} [2m^4(\hat{t} - m_Z^2) + m^2(2m_Z^4 + (\hat{s} + 6\hat{t})m_Z^2 - 2\hat{t}(\hat{s} + 4\hat{t})) \right. \\
& + \hat{t}(2\hat{t}(\hat{s} + \hat{t}) - m_Z^2(\hat{s} + 2\hat{t}))] + \frac{g_v\kappa_g\kappa_z}{\hat{t}} [2m_Z^2(m^2 - \hat{t}) + \hat{t}(m^2 - \hat{u})] \\
& + \frac{\kappa_g^2(m^2 - \hat{t})(g_v^2 + g_a^2)}{\hat{t}^2} [m^2(\hat{t}^2 - 2m_Z^4) - \hat{t}(\hat{t}(\hat{t} + \hat{u}) - m_Z^2(\hat{t} + 2\hat{u}))] \\
& + \frac{2\kappa_g^2\hat{s}(m^2 - \hat{s})}{9m_Z^2\hat{t}[(\hat{s} - m^2)^2 + \Gamma^2 m^2]} [9(g_v^2 + g_a^2)((\hat{t} - m^2)(2m_Z^2 - m^2\hat{t}) - \hat{s}\hat{t}m^2) \\
& + 4s_W^2\hat{s}(4s_W^2 - 3)\hat{t}^2] + \frac{2\kappa_z^2}{\hat{s}(\hat{t} - m^2)} [m^2(\hat{s} - m^2)(2\hat{t} - m_Z^2) + m_Z^2(m^2(\hat{t}^2 + m^2) \\
& + \hat{t}\hat{s} - \hat{u}m_Z^2)] + \frac{\kappa_z\kappa_g g_v}{\hat{t}(\hat{t} - m^2)} [(m_Z^2 - \hat{t})(6m^4 - 11\hat{t}m^2 + 5\hat{t}^2) + \hat{s}\hat{t}(3m^2 - \hat{t})] \quad (5) \\
& + \frac{\kappa_z\kappa_g g_v(\hat{s} - m^2)}{(\hat{t} - m^2)[(\hat{s} - m^2)^2 + \Gamma^2 m^2]} [3m^4(\hat{u} - m^2) - \hat{s}(\hat{s}(3m^2 - \hat{t}) + 3m_Z^2(\hat{t} - m^2)) \\
& \left. - \hat{t}(\hat{t}(3m^2 - \hat{s}) + m^2(10\hat{s} - 3m_Z^2))] \right] + [\hat{t} \leftrightarrow \hat{u}] \Big\}
\end{aligned}$$

where g_v and g_a are the vector and axial-vector couplings of the weak neutral current; m_Z is the mass of the Z boson.

-
- [1] H.-J. He, N. Polonsky, S. Su, Phys. Rev. D **64**, 053004 (2001) [hep-ph/0102144].
 - [2] J. Erler and P. Langacker, Phys. Rev. Lett. **105**, 031801 (2010).
 - [3] K. Nakamura *et al.*, (Particle Data Group), Journal of Physics G **37**, 075021 (2010).
 - [4] J. Conway *et al.*, CDF Collaboration, CDF Note 10110, (2010).

- [5] T. Aaltonen *et al.*, CDF Collaboration, Phys. Rev. Lett. **104**, 091801 (2010); arXiv:0912.1057 [hep-ex].
- [6] M.S. Chanowitz, M.A. Furman and I. Hinchliffe, Phys. Lett. B **78**, 285 (1978); Nucl. Phys. B **153**, 402 (1979); M.S. Chanowitz, Phys. Rev. D **82**, 035018 (2010).
- [7] G.D. Kribs *et al.*, Phys. Rev. D **76**, 075016 (2007), arXiv:0706.3718 [hep-ph].
- [8] B. Holdom *et al.*, PMC Physics A **3**, 4 (2009); [arXiv:0904.4698].
- [9] W. S. Hou and C. Y. Ma, Phys. Rev. D **82**, 036002 (2010).
- [10] S. Bar-Shalom, D. Oaknin and A. Soni, Phys. Rev. D **80**, 015011 (2009).
- [11] A. J. Buras *et al.*, JHEP **1009**, 106 (2010).
- [12] A. Soni *et al.*, Phys. Lett. B **683**, 302 (2010).
- [13] O. Eberhardt, A. Lenz and J. Rohrwild, Phys. Rev. D **82**, 095006 (2010).
- [14] A. Soni *et al.*, Phys. Rev. D **82**, 033009 (2010).
- [15] A. K. Alok, A. Dighe and D. London, Phys. Rev. D **83**, 073008 (2011).
- [16] B. Holdom, Phys. Rev. Lett. **57**, 2496 (1986) [Erratum-ibid. **58**, 177 (1987)].
- [17] C. T. Hill, M. A. Luty and E. A. Paschos, Phys. Rev. D **43**, 3011 (1991).
- [18] T. Elliott and S. F. King, Phys. Lett. B **283**, 371 (1992).
- [19] P. Q. Hung and C. Xiong, Nucl. Phys. B **848**, 288 (2011).
- [20] B. Holdom, JHEP **0608**, 076 (2006).
- [21] P. Q. Hung and M. Sher, Phys. Rev. D **77**, 037302 (2008).
- [22] P. Q. Hung, C. Xiong, Phys. Lett. B **694**, 430-434 (2011).
- [23] P. Q. Hung and C. Xiong, Nucl. Phys. B **847**, 160 (2011).
- [24] A.Senol, A.T. Tasci and F. Ustabas, Nucl.Phys. B **851**, 289 (2011); arXiv:1104.5316 [hep-ph].
- [25] A. T. Alan, A. Senol and O. Cakir, Europhys. Lett. **66**, 657-660 (2004).
- [26] O. Cakir, A. Senol and A. T. Tasci, Europhys. Lett. **88**, 11002 (2009); O. Cakir and V. Cetinkaya, Mod. Phys. Lett. A **25**, 2571 (2010).
- [27] M. Sahin, S. Sultansoy and S. Turkoz, Phys. Rev. D **82**, 051503 (2010); M. Sahin, S. Sultansoy and S. Turkoz, Phys. Rev. D **83**, 054022 (2011).
- [28] I. T. Cakir *et al.*, Phys. Rev. D **80**, 095009 (2009).
- [29] R. Ciftci, Phys. Rev. D **78**, 075018 (2008).
- [30] O. Cakir *et al.*, Eur. Phys. J. C **56**, 537 (2008).
- [31] E.Boos *et al.*, [CompHEP Collaboration], Nucl. Instrum. Meth. A **534**, 250 (2004).

[32] J. Pumplin *et al.*, JHEP **07**, 012 (2002).

[33] W. S. Y. Hou, M. Nagashima and A. Soddu, Phys. Rev. D **76**, 016004 (2007).